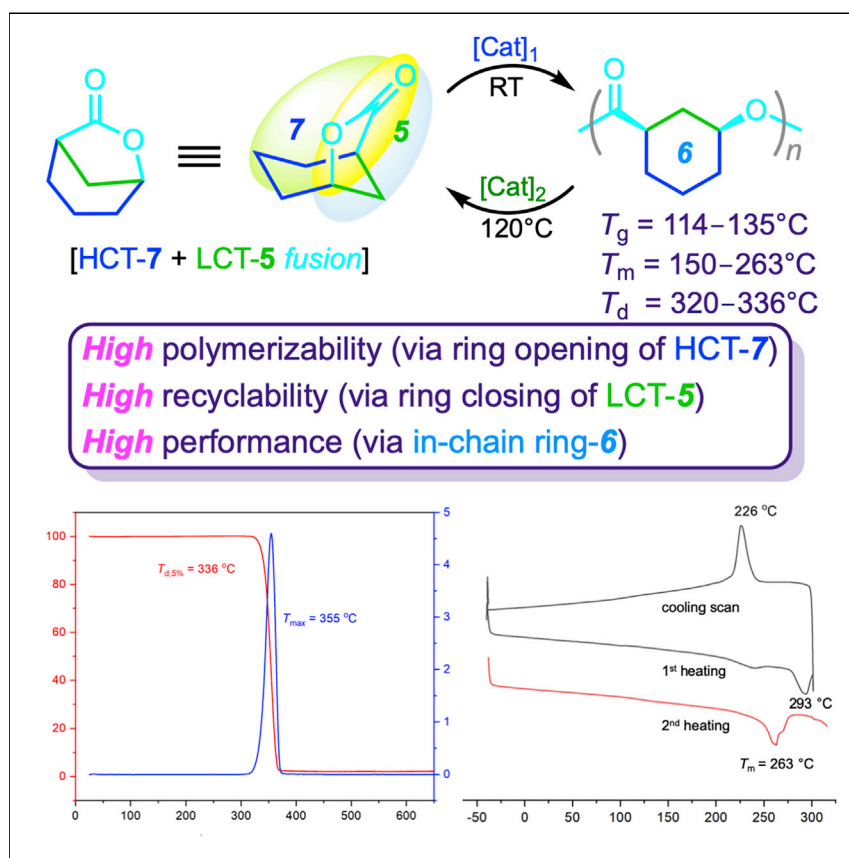


Article

Hybrid monomer design for unifying conflicting polymerizability, recyclability, and performance properties



Hybrid monomer design is shown to be a powerful approach to develop robust circular plastics without yielding to common property trade-offs by hybridizing parent monomer structures to an offspring monomer that can unify conflicting (de) polymerizability and performance properties.

Changxia Shi, Zi-Chen Li, Lucia Caporaso, Luigi Cavallo, Laura Falivene, Eugene Y.-X. Chen

lafalivene@unisa.it (L.F.)
eugene.chen@colostate.edu (E.Y.-X.C.)

HIGHLIGHTS

Circular plastics can be designed with high-performance properties

Hybrid monomer design radically alters properties of the resulting recyclable polymers

Property trade-offs can be overcome by hybridizing low/high ceiling temperature monomers

Article

Hybrid monomer design for unifying conflicting polymerizability, recyclability, and performance properties

Changxia Shi,^{1,2} Zi-Chen Li,² Lucia Caporaso,³ Luigi Cavallo,⁴ Laura Falivene,^{3,*} and Eugene Y.-X. Chen^{1,5,*}

SUMMARY

Intrinsically recyclable polymers represent a circular economy approach to address plastics problems. However, the design of such circular polymers is challenged by unyielding trade-offs between the monomer's polymerizability and the polymer's depolymerizability and performance properties. Here, we introduce a hybrid monomer design strategy that synergistically couples a high ceiling temperature (HCT) sub-structure for high polymerizability and performance properties with a low ceiling temperature (LCT) sub-structure for high depolymerizability and recyclability within the same monomer structure. Thus, structural hybridization between HCT ϵ -caprolactone and LCT γ -butyrolactone led to an offspring [3.2.1]bicyclic lactone, which exhibits both high polymerizability and depolymerizability, otherwise conflicting properties in a typical monomer. The resulting polymer becomes a high-performance material, and thermal transition temperatures are $\sim 200^\circ\text{C}$ higher and tensile modulus 10 \times higher than its parent polymers. These results demonstrate that the HCT/LCT hybrid monomer strategy is a powerful approach for designing circular polymers where conflicting properties must be exploited and unified.

INTRODUCTION

The current largely unsustainable plastics manufacturing, consumption, and disposal schemes have caused alarming plastics problems associated with their environmental pollution as well as tremendous energy and materials value loss in the economy.^{1–4} Among several approaches being explored^{5–16} to combat such problems, the development of next-generation, chemically recyclable polymers^{17–33} promises a circular plastics economy approach to address these complex issues.^{34–36} Monomer design^{37,38} is the cornerstone of discovering new circular polymers with intrinsic chemical recyclability, the design of which requires to overcome typical trade-offs between monomer's polymerizability and polymer's depolymerizability, as well as between polymer's recyclability and performance, until a practically useful balance is struck. These stringent thermodynamic, kinetic, and real-world performance requirements present a formidable challenge for developing circular plastics that exhibit not only full chemical recyclability but also high-performance properties. Nevertheless, notable advances have been achieved toward that ultimate goal. For example, the ring-opening polymerization (ROP) of low ceiling temperature (LCT), "nonstrained" five-membered γ -butyrolactone (γ -BL) led to poly(γ -butyrolactone) (PGBL) that can be completely depolymerized back to γ -BL in high (>99%) purity and yield with a low energy input.^{39,40} The limited stability and mechanical performance properties

The bigger picture

Synthetic polymers have become indispensable for modern life and the global economy. However, the manufacturing and disposal of most of today's polymers follow a linear economy model, which has caused accelerated depletion of finite natural resources, severe worldwide plastics pollution, and enormous materials value loss. The design of future circular polymers considers closed-loop lifecycles toward a circular economy. A key challenge of this promising design includes innovation in monomer structure that could enable not only efficient polymerization to polymers with properties comparable to today's polymers but also selective depolymerization to recover the monomers with high yield and purity. However, these contrasting properties are conflicting in a single monomer structure. This work introduces a hybrid monomer design concept that hybridizes contrasting parent monomer structures to an offspring monomer that can unify conflicting (de)polymerizability and performance properties.



of PGBL have been subsequently addressed by *trans*-fusion of a cyclohexyl ring to the γ -BL core, affording a fused bicyclic lactone monomer that led to much-enhanced monomer polymerizability as well as better polymer thermal stability and crystallinity while maintaining the full chemical recyclability as a circular plastic.^{21,22} However, the resulting highly crystalline polymer is a brittle material, and to increase its ductility as a packaging material, synthesizing a copolymer with a sufficient amount of the flexible PGBL incorporated was required.⁴¹ Another notable set of designer monomers for circular plastics is a class of bridged bicyclic thiolactone monomers such as chiral N-substituted *cis*-4-thia-L-proline thiolactones²⁵ and 2-thiabicyclo[2.2.1]heptan-3-one (^[221]BTL).⁴² The bridged bicyclic framework locks the monomer structure in the *cis*-configuration, thus rendering the chemical recyclability and depolymerization selectivity. The classic Thorpe-Ingold effect through gem-disubstitution has also been exploited in the β -butyrothiolactone monomer design to enable the chemical recyclability.⁴³ Here, it is worth noting that the chemistry of the analogous lactones is notably different than the above thiolactones. For example, replacing the S atom in ^[221]BTL with the O atom gives the bicyclic lactone congener, which leads to a polyester that is atactic, amorphous, and not recyclable—essentially the opposite of the properties of the polythioester.⁴²

Thus, it remains a challenging task to combine several desired, but conflicting, properties into one lactone monomer. As copolymerization of two or more different monomers is considered as an effective strategy to obtain the materials with tailored properties by adjusting the chemical nature, composition, and sequence of the comonomers, often delivering improved or unattainable properties in relation to those of the constituent homopolymers,^{44–51} it thus became an attractive strategy to address the trade-off issues. In this context, the LCT γ -BL was copolymerized with high ceiling temperature (HCT) and strained seven-membered ϵ -caprolactone (ϵ -CL)^{52,53} to produce copolymers aimed for enhanced polymerizability and thermal stability for PGBL, and degradability and recyclability for poly(ϵ -caprolactone) (PCL).^{54–57} However, over the entire copolymer composition range, the glass-transition temperature (T_g , from -48°C to -65°C) and melting-transition temperature (T_m , from 11°C to 63°C) of the copolymers are still low and confined within the values of their parent homopolymers (Figure 1A).⁵⁸ Most recently, the comonomer strategy has been utilized to render degradability and recyclability of thermosets via incorporation of a cleavable comonomer.⁵⁹ Whereas copolymerization can be employed as an effective strategy to mitigate the trade-offs, increasing speciation can complicate the chemical recycling and the copolymer properties are often still confined within those of constituent homopolymers.⁵⁸

Hybridization is a common phenomenon found in chemistry and biology, the process of which combines the qualities of different varieties or species of parents to produce offspring that can be distinctively or radically different than the parents. Applying this general hybridization principle, here we introduce a hybrid monomer design strategy that synergistically couples a HCT sub-structure for high polymerizability and performance properties with a LCT sub-structure for high depolymerizability and recyclability within the same monomer structure. To demonstrate the uniqueness and effectiveness of this strategy for circular polymer design where conflicting properties must be balanced or exploited, herein we describe that structural hybridization between the HCT ϵ -CL and the LCT γ -BL leads to an offspring [3.2.1] bicyclic lactone (BiL), 6-oxabicyclo[3.2.1]octan-7-one, which can be synthesized from 3-cyclohexene-1-carboxylic acid via a two-step reaction in a relatively large laboratory scale (80 g) and high yield ($\sim 92\%$ isolated overall yield) (Figure 1B). We hypothesized that this hybrid monomer structure could bring about an intriguing

¹Department of Chemistry, Colorado State University, Fort Collins, CO 80523-1872, USA

²Beijing National Laboratory for Molecular Sciences, Key Laboratory of Polymer Chemistry and Physics of Ministry of Education, Center for Soft Matter Science and Engineering, College of Chemistry & Molecular Engineering, Peking University, Beijing 100871, China

³Università di Salerno, Dipartimento di Chimica e Biologia, Via Papa Paolo Giovanni II, 84100 Fisciano, SA, Italy

⁴King Abdullah University of Science and Technology (KAUST), Physical Sciences and Engineering Division, KAUST Catalysis Center, Thuwal 23955-6900, Saudi Arabia

⁵Lead contact

*Correspondence: lafalivene@unisa.it (L.F.), eugene.chen@colostate.edu (E.Y.-X.C.)

<https://doi.org/10.1016/j.chempr.2021.02.003>

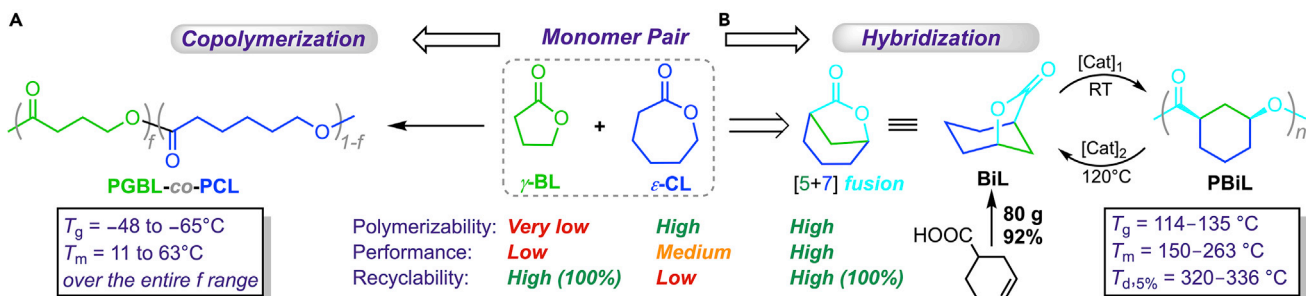


Figure 1. Hybrid monomer design versus conventional copolymerization approach

(A) Conventional comonomer copolymerization approach.
(B) Structural hybridization approach reported in this work.

divergent polymerization/depolymerization pathway scenario where the polymerization proceeds as if via the ring-opening of the HCT sub-structure and the depolymerization occurs as if through the ring-closing to form the LCT sub-structure (Figure 1B), thereby achieving both high polymerizability and depolymerizability, otherwise conflicting properties in a typical monomer. We further reasoned that the ROP of one ring in the bicyclic BiL will keep the other ring intact, thus leading to an intriguing ring-containing (in-chain) polyester, and that incorporation of the in-chain aliphatic rings could enhance the thermal properties of the resulting polymer because of increased backbone rigidity.^{21,60,61} Furthermore, the resulting polymer exhibits two stereogenic centers in a repeat unit, which presents a number of possible stereo-microstructures or tacticities and, thus, the opportunity to use polymer stereochemistry controllable by catalysts or initiators to tune materials properties.

Indeed, BiL can be readily polymerized under ambient conditions to high-molecular-weight poly(BiL) (PBiL) materials that exhibit both high-performance properties and complete chemical recyclability. Most remarkably, PBiL displays a high T_g up to 135°C and T_m up to 263°C, which are ~200°C higher than both T_g and T_m values of the parent homopolymers (PGBL and PCL) and their copolymers (Figure 1B). In addition, mechanical properties of PBiL, particularly Young's modulus, are ~10x higher than its parent polymers, demonstrating that the HCT/LCT hybrid monomer strategy is a powerful approach for designing circular polymers and delivering radically different or much-enhanced properties over the parent homopolymers or copolymers.

RESULTS

Suppressing epimerization to achieve exclusive stereoretention ROP

The hybrid atom-bridged bicyclic BiL is locked in a *cis*-configuration whereas a *trans*-configurational isomer is not possible in its monomer state. Upon the ROP, however, the resulting polymer PBiL can adopt either a *cis* (stereoretention) or *trans* (epimerization) configurational structure, or both. Hence, our first objective was to examine whether the ROP retains the *cis*-configuration or undergoes epimerization to form a *trans* structure and possible effects of the catalyst or mechanism on the stereoretention versus epimerization dynamics. To this end, we probed the ROP characteristics employing both organocatalyzed^{62–64} and metal-catalyzed coordination-insertion mechanisms.^{65,66}

As triazabicyclodecene (TBD) has been shown to be one of the most active and efficient organic catalysts for the ROP of lactones,^{67,68} at the outset, we investigated characteristics of the ROP of BiL with TBD. The TBD-catalyzed ROP in toluene (6.0 M) at room temperature (RT, ~23°C) with [BiL]/[TBD]/[BnOH] = 600/3/1 (BnOH = benzyl alcohol as the

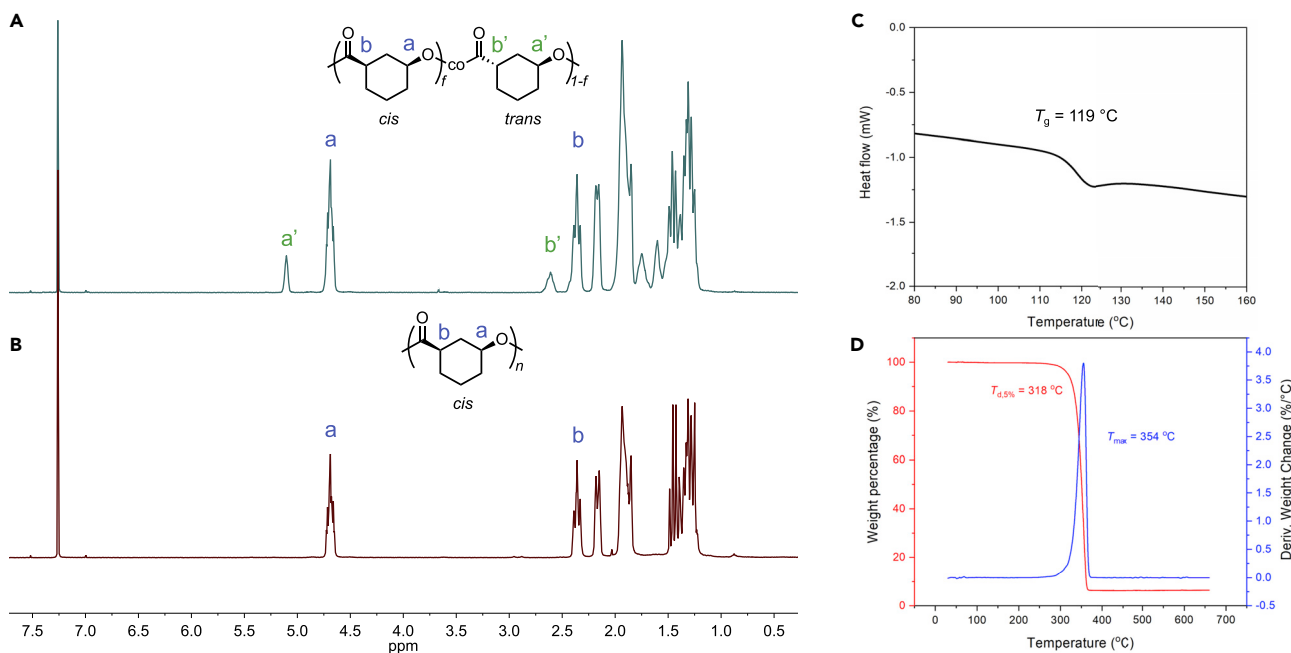


Figure 2. ^1H NMR ($23\text{ }^\circ\text{C}$, CDCl_3) spectra and thermal properties of PBiL produced by organopolymerization

- (A) PBiL produced by TBD ($[\text{BiL}]/[\text{TBD}]/[\text{BnOH}] = 600/3/1$) containing 18% *trans* isomer (derived from epimerization).
- (B) A reference PBiL produced by metal-catalyzed ROP (stereoretention polymer product without epimerization) with La-1 ($[\text{BiL}]/[\text{La-1}] = 100/1$).
- (C) DSC (from a second heating scan at $10\text{ }^\circ\text{C min}^{-1}$) thermogram of PBiL ($M_n = 56.7\text{ kg mol}^{-1}$) by TBD.
- (D) TGA and DTG (at $10\text{ }^\circ\text{C min}^{-1}$ heating scan) thermograms of PBiL ($M_n = 56.7\text{ kg mol}^{-1}$) by TBD.

initiator) achieved 95% conversion after 48 h. The resulting polymer PBiL had a medium number-average molecular weight (M_n) of 56.7 kg mol^{-1} but the dispersity (D) was relatively broad ($D = 1.22$). NMR studies of the PBiL produced by TBD showed that epimerization at the carbon stereogenic center adjacent to the carbonyl carbon took place during the ROP, thus affording the PBiL containing both *cis* (82%) and *trans* (18%) stereoconfigurations (Figure 2A). More specifically, the ^1H NMR spectrum exhibited two sets of peaks at both the alkoxy methine proton [$-\text{CHO}-$] region (labels *a* and *a'* for *cis* and *trans* configurations, respectively) and the acyl methine proton [$-\text{CHC}(\text{C=O})-$] region (labels *b* and *b'* for *cis* and *trans* configurations, respectively). This finding is consistent with reports that strongly nucleophilic and basic TBD often causes side reactions during polymerization, such as transesterification and epimerization.⁶⁹ As a result, the resulting PBiL is an amorphous material but displays a high glass-transition temperature (T_g) of $119\text{ }^\circ\text{C}$, as determined by differential scanning calorimetry (DSC) (Figure 2C). This T_g value represents $\sim 170\text{ }^\circ\text{C}$ - $180\text{ }^\circ\text{C}$ enhancements in T_g in relation to homopolymers PGBL and PCL as well as their copolymers. Noteworthy also is that it exhibits a high decomposition temperature ($T_{d,5\%$ }, defined by the temperature at 5% weight loss) of $318\text{ }^\circ\text{C}$ and a high maximum rate decomposition temperature (T_{max}) of $354\text{ }^\circ\text{C}$, as measured by thermogravimetric analysis (TGA) and derivative thermogravimetric analysis (DTG) (Figure 2D). This T_d value is about $116\text{ }^\circ\text{C}$ higher than that of PGBL and similar to that of PCL.

To suppress or eliminate epimerization during polymerization, next, we turned our attention to the metal-mediated coordination-insertion mechanism by metal complexes bearing a vacant coordination site for binding thus activating the monomer and a nucleophilic ligand for initiating the polymerization.^{65,66} As a start, we first employed La $[\text{N}(\text{SiMe}_3)_2]_3$ (La-1), as it is commercially available and has been shown to be highly effective for catalyzing coordination-insertion ROP of lactones³⁹ and also leading to cyclic

Table 1. Results of ROP of BiL by different metal catalyst/initiator systems

Run no.	Catalyst no.	[BiL]/[Cat] /[I]	Time (h)	Conv. ^a (%)	M_n (calcd) ^b (kg mol ⁻¹)	M_n ^c (kg mol ⁻¹)	D ^c (M_w/M_n)	I^d (%)	Tacticity ^e (P_m)
1	La-1	300/1/3	8	92	11.7	13.1	1.10	90	0.35
2	rac-La-2	200/1/1	3	91	23.1	27.5	1.03	84	0.34
3	rac-La-2	1,000/1/1	12	93	117	94.3	1.06	124	0.38
4	rac-La-2	1,500/1/1	12	89	168	153	1.06	110	0.36
5	rac-Y-1	100/1/1	12	93	11.8	12.0	1.07	98	0.46
6	rac-Y-1	1,000/1/1	16	52	65.6	59.2	1.05	111	0.52
7	rac-Y-2	100/1/1	12	86	11.0	13.4	1.05	82	0.34
8	rac-Y-3	100/1/1	72	89	11.3	10.4	1.05	84	0.42
9 ^f	rac-Y-3	100/1/1	72	87	11.1	9.90	1.06	112	0.44
10	(S,S)-Y-3	100/1/1	48	65	8.43	8.90	1.06	95	0.74
11 ^f	(S,S)-Y-3	100/1/1	48	52	6.67	6.70	1.05	100	0.85
12 ^g	(S,S)-Y-3	100/1/1	48	46	5.92	5.60	1.09	106	0.87

Conditions: $[BiL]_0 = 6.0$ M, toluene, RT, initiator (I) = BnOH (except runs 9, 11, and 12).

^aMonomer conversions measured by ¹H NMR of the quenched solution in benzoic acid/chloroform.(+)-1-Phenylethanol as initiator.

^b M_n (calculated) = $([BiL]_0/[I]_0) \times conv.\% \times (\text{molecular weight of BiL}) + (\text{molecular weight of I})$.

^cWeight-average molecular weights (M_w), number-average molecular weights (M_n), and dispersity indices ($D = M_w/M_n$) determined by GPC at 40°C in CHCl₃ coupled with a DAWN HELEOS II multi (18)-angle light scattering detector and an Optilab TrEX dRI detector for absolute molecular weights.

^dInitiation efficiency (I^*) = $M_n(\text{calcd})/M_n(\text{exptl})$.

^eMeasured by ¹³C NMR in the carbonyl region with P_m percentages relative to the *cis/cis* diisotactic peak at 174.0 ppm established by the enantiomerically pure monomer.

^f(R)-(+)-1-Phenylethanol as initiator.

^g(S)-(−)-1-Phenylethanol as initiator.

polyesters when used in the absence of an alcohol co-initiator.²¹ The effectiveness of La-1 toward the ROP of BiL was examined with a [BiL]/[La-1] ratio of 100/1 in toluene, achieving 96% conversion at RT after 24 h. Importantly, the PBiL produced by the metal-catalyzed coordination-insertion ROP completely returned the *cis*-configuration without noticeable racemization on the basis of ¹H NMR analysis (Figures 2B versus 2A). Specifically, the ¹H NMR spectrum of the PBiL produced by La-1 displayed no peaks associated with the *trans* configuration (i.e., a'- and b'-labeled peaks attributed to epimerization, Figure 2B). When combined with the co-initiator BnOH that converts instantaneously the silylamide precatalyst to the alkoxide catalyst *in situ*,³⁹ the polymerization at RT in toluene with [BiL]/[La-1]/[BnOH] = 300/1/3 achieved 92% conversion after 8 h (run 1, Table 1). The resulting polymer had a narrower dispersity of $D = 1.10$ as compared with the TBD-derived PBiL.

The ROP of BiL by the [La-1] + [BnOH] system is well-controlled, as evidenced by the following four lines of evidence. First, the ROP followed strictly first-order kinetics ($R^2 = 0.993$) up to high conversions (Figure 3A). Second, the molecular weight increased linearly with monomer conversion whereas the dispersity of the resulting PBiL remained low ($D < 1.1$) (Figure 3B). Third, the absolute molecular weight of the isolated PBiL at 92% conversion was measured by a gel-permeation chromatography (GPC) instrument equipped with multi (18)-angle light scattering and dRI (differential refractive index) detectors to have a M_n of 13.1 kg mol⁻¹; this measured M_n is close to the calculated M_n of 11.7 kg mol⁻¹ based on the [BiL]/[I] ratio, thus giving a high initiation efficiency of 90% (run 1, Table 1). Furthermore, this measured M_n is essentially identical to the calculated M_n of 13.9 kg mol⁻¹ based on the chain ends of PBiL characterized by ¹H NMR (Figure S5), which also revealed a linear chain structure and showed high end-group fidelity. Fourth, the BnOH-initiated linear structure with only the predicted end groups, BnO-[BiL]_n-H, was confirmed by matrix-assisted laser desorption/ionization time-of-flight mass spectrometry (MALDI-TOF MS) by using a low molecular weight sample prepared with [BiL]/[La-1]/

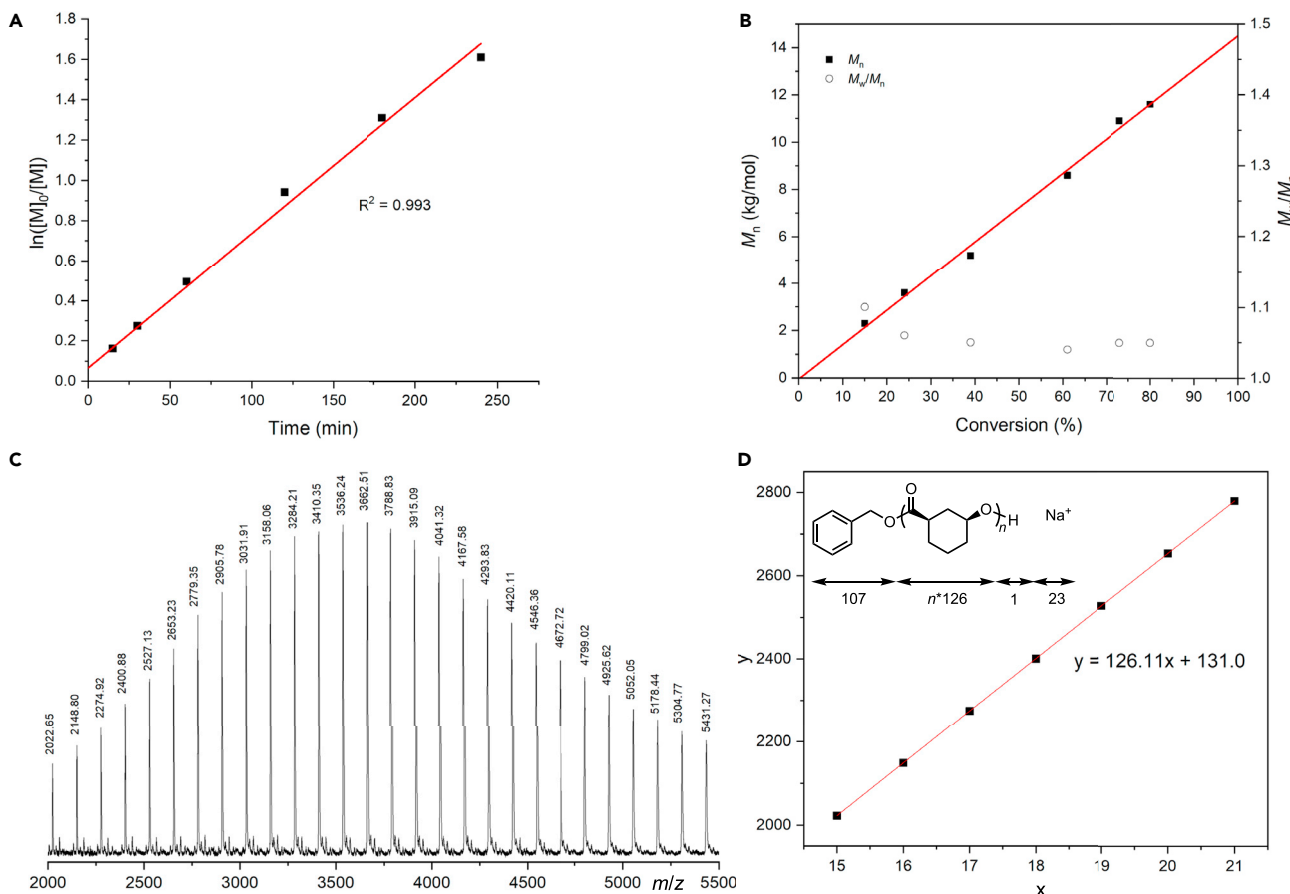


Figure 3. ^1H NMR (23°C , CDCl_3) spectra and thermal properties of PBiL by metal-catalyzed stereoretention ROP

(A) Semilogarithmic kinetic plot of the ROP with $[\text{BiL}]/[\text{La-1}]/[\text{BnOH}] = 300/1/3$ ($[\text{BiL}]_0 = 6.0 \text{ M}$, toluene, RT).

(B) Plots of M_n and D values versus BiL conversion.

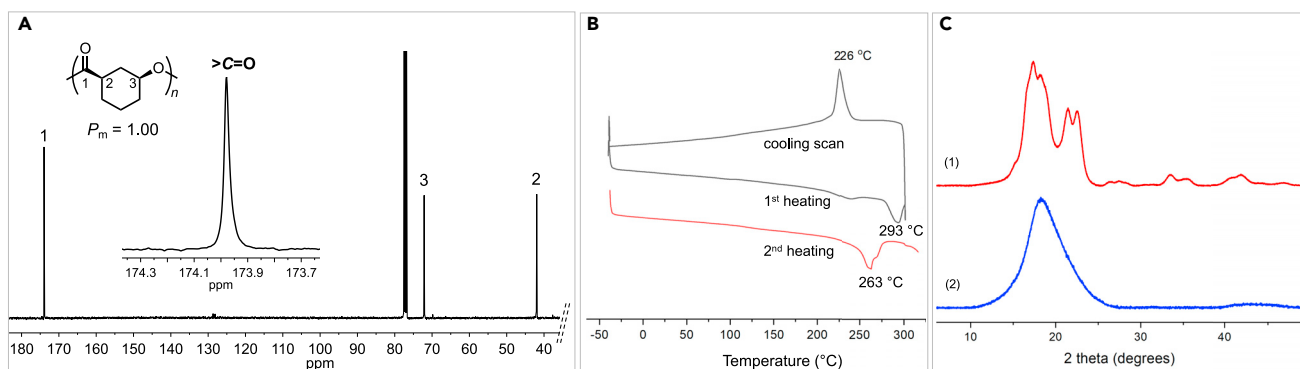
(C) MALDI-TOF MS spectrum of the PBiL produced with $[\text{BiL}]/[\text{La-1}]/[\text{BnOH}] = 100/1/3$.

(D) Plot of m/z values (y) versus the theoretical number of BiL repeat units (x).

$[\text{BnOH}] = 100/1/3$ (Figure 3C). Specifically, the MS spectrum consisted of only one series of molecular ion peaks, and the spacing between the two neighboring molecular ion peaks was that of the exact molar mass of the repeat unit ($m/z = 126.15$), as shown by the slope (126.11) of the linear plot of m/z values (y) versus the number of BiL repeat units (x) (Figure 3D). The intercept of the plot, 131.0, represents the total mass of chain ends + that of Na^+ [$108.14 (\text{BnO}/\text{H}) + 23.0 (\text{Na}^+) \text{ g mol}^{-1}$].

Pure isotactic polymer from (1R, 5S)-BiL and isotactic polymer from rac-BiL

The above described exclusive stereoretention ROP enabled by the metal-catalyzed coordination-insertion ROP offers the opportunity to produce perfectly isotactic PBiL starting from a chiral monomer, (1R, 5S)-6-oxabicyclo[3.2.1]octan-7-one [(1R, 5S)-BiL], synthesized from commercial reagent (*R*)-(+)3-cyclohexenecarboxylic acid. The ROP with $[(1R, 5S)\text{-BiL}]/[\text{La-1}]/[\text{BnOH}] = 500/1/3$ yielded the corresponding chiral polymer P[(1R, 5S)-BiL] with $[\alpha]_{589}^{22.4} = -70 \text{ deg dm}^{-1} \text{ g}^{-1} \text{ cm}^3$ in CHCl_3 , $M_n = 19.3 \text{ kg mol}^{-1}$, and $D = 1.08$ at 94% conversion. The calculated theoretical M_n based on the $[\text{BiL}]/[\text{I}]$ ratio is 21.1 kg/mol, which is close to both the values measured by GPC and by ^1H NMR ($M_n = 22.5 \text{ kg mol}^{-1}$) (Figure S7), indicating a near quantitative initiation efficiency and chain-end fidelity. The resulting polymer is a pure isotactic material, displaying no stereoerrors on its ^{13}C NMR ($P_m = 1.00$) (Figures 4A and S8). This chiral

**Figure 4.** Pure isotactic polymer from (1*R*, 5*S*)-BiL(A) ^{13}C NMR (23°C , CDCl_3) spectrum of P[(1*R*, 5*S*)-BiL] prepared with $[(1R, 5S)\text{-BiL}]/[\text{La-1}]/[\text{BnOH}] = 500/1/3$ (6.0 M, toluene, RT).(B) DSC thermograms of P[(1*R*, 5*S*)-BiL] from first heat, cooling, and second heating scans at $10^\circ\text{C min}^{-1}$.(C) pXRD profiles of semi-crystalline P[(1*R*, 5*S*)-BiL] (1) and reference amorphous PBiL derived from rac-BiL by La-1 + BnOH (2).

polymer exhibited a remarkably high T_m of 293°C on the DSC first heating scan or 263°C on the second heating scan with a crystallization temperature of 226°C but no observable T_g (Figure 4B). The semi-crystalline nature of this polymer was further confirmed by its powder X-ray diffraction (pXRD) profile, featuring sharp diffraction peaks at 2θ values of 17.3° , 18.3° , 21.5° , and 22.5° , in relation to an atactic, amorphous reference PBiL sample produced from rac-BiL by La-1 + BnOH (Figure 4C). By using La-1 alone without the alcohol co-initiator, a chiral cyclic polymer with an ultra-high M_n of over 1 million Da ($1,100 \text{ kg mol}^{-1}$, $D = 1.35$) was prepared, which accordingly exhibited no end groups (Figure S9) and stereoerrors (Figure S10).

When rac-BiL was polymerized by achiral catalyst La-1, only iso-enriched PBiL was produced with a low isotacticity of $P_m = 0.35$ (Figure S6). To improve the stereoselectivity of the ROP of rac-BiL, we next employed discrete chiral yttrium and lanthanum complexes supported by C_2 -symmetric salen ligands (Figure 5A) as such catalysts have been shown to mediate highly stereoselective polymerization of eight-membered rac-diolides.^{44,45,70} The use of rac-La-2 supported by the sterically demanding salcy ligand with bulky CPh₃ substituents at the 3-positions of the ligand rendered much more active polymerization system but the isotacticity of PBiL remained essentially the same (runs 2–4, Table 1). However, the high activity of rac-La-2/BnOH enabled the synthesis of high-molecular-weight linear PBiL ($M_n = 153 \text{ kg mol}^{-1}$, $D = 1.06$, run 4, Table 1) by employing a high ratio of [BiL]/[rac-La-2]/[BnOH] = 1,500/1/1. This PBiL is an amorphous material exhibiting the highest T_g (135°C) of the series (Figure 5C).

Moving to a metal center with a smaller ionic radius, rac-Y-1 with 3,5-CMe₃ substituents on the salcy ligand brought about the ROP with a nearly perfect initiation efficiency (98%) and, more significantly, considerably enhanced isotacticity ($P_m = 0.4$, run 5, Table 1) with [BiL]/[rac-Y-1]/[BnOH] = 100/1/1. Increasing this ratio to 1,000/1/1 afforded PBiL with $M_n = 59.2 \text{ kg mol}^{-1}$, $D = 1.05$, and $P_m = 0.52$ (run 6, Table 1). As expected, this PBiL is still an amorphous material with $T_g = 128^\circ\text{C}$. We also examined effects of solvent polarity [toluene, tetrahydrofuran (THF), dichloromethane], [BiL]/[rac-Y-1] ratio (50/1 to 300/1), and [BiL] concentration (3.0 to 12 M) on polymerization characteristics (Table S1). Based on the results summarized in Table S1, several trends can be observed. Although the ROP was fastest in THF, the resulting PBiL exhibited the broadest dispersity (D up to 1.18). In contrast, the ROP carried out in toluene had a moderate polymerization rate, but it produced PBiL with the narrowest dispersity. However, the tacticity of the polymer was not noticeably affected by the above variations.

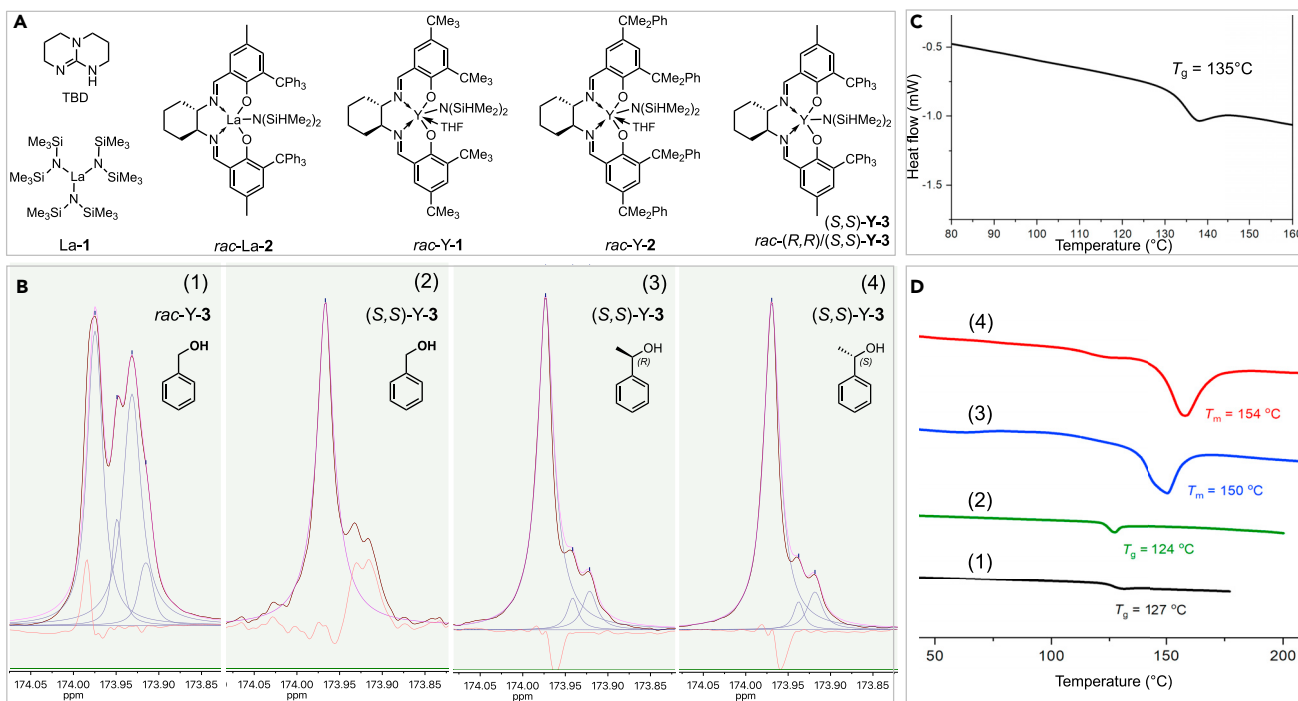


Figure 5. Iso-rich and isotactic polymers from rac-BiL

(A) Chemical structures of the catalysts employed in this study.

(B) ^{13}C NMR (25°C , CDCl_3) spectra in the carbonyl region of iso-rich (1, 2) and isotactic (3, 4) PBiL samples by racemic and enantiopure Y-3 catalysts in combination with achiral and chiral alcohols: (1) $P_m = 0.42$ (run 8, Table 1); (2) $P_m = 0.74$ (run 10, Table 1); (3) $P_m = 0.85$ (run 11, Table 1); and (4) $P_m = 0.87$ (run 12, Table 1).

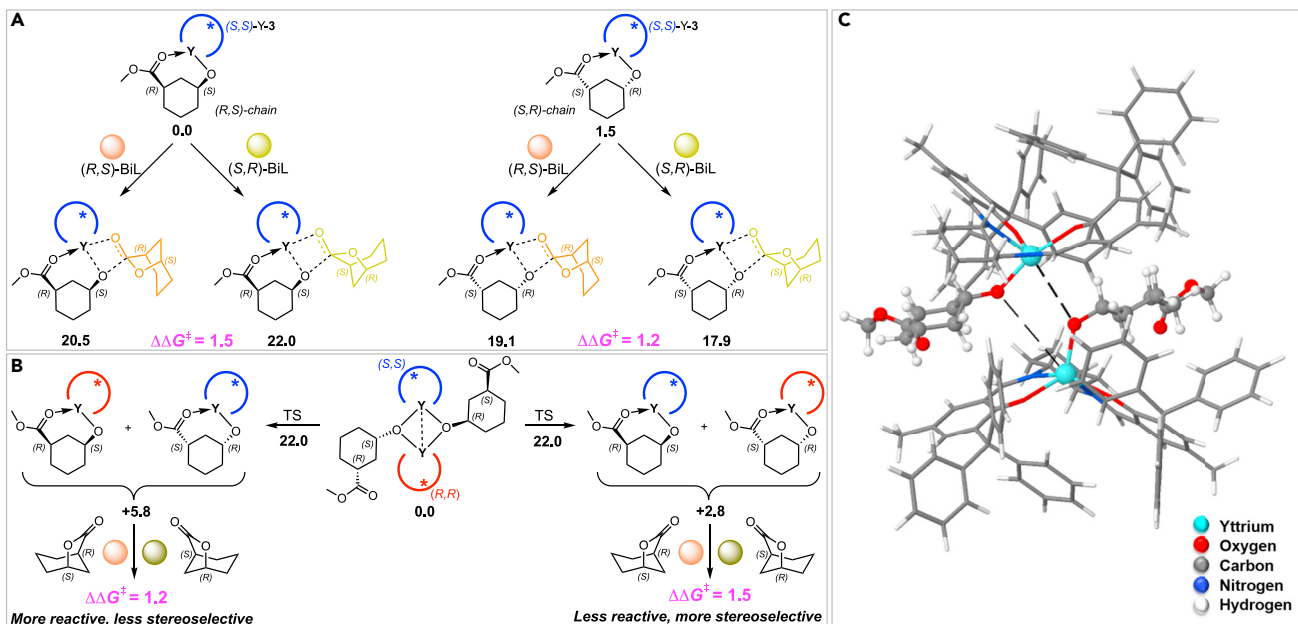
(C) DSC thermogram of the iso-rich, amorphous PBiL ($M_n = 153 \text{ kg mol}^{-1}$, $D = 1.06$) by *rac*-La-2.

(D) DSC thermograms of PBiL materials with varied isotacticity by racemic and enantiopure Y-3 catalysts: (1) $P_m = 0.42$; (2) $P_m = 0.74$; (3) $P_m = 0.85$; (4) $P_m = 0.87$.

Further increasing the ligand steric bulk by introducing bulkier 3,5-CMe₂Ph substituents (*rac*-Y-2) and 3-CPh₃-5-Me substituents (*rac*-Y-3) to the salcy ligand did not further increase the isotacticity (runs 7 and 8, Table 1). Replacing the BnOH co-initiator with chiral alcohol, (*R*)(+)-1-phenylethanol, as initiator also did not noticeably affect the tacticity (run 9, Table 1). These results suggest the large number of stereoerrors generated by these racemic catalysts could be originated from polymer chain exchange⁷¹ between two antipodal catalyst centers (*vide infra*). To test this hypothesis, we employed enantiomeric pure catalyst (S,S)-Y-3 and indeed observed a substantial increase in the polymer isotacticity to $P_m = 0.74$ (run 10, Table 1). When this enantiomeric catalyst was combined with a chiral alcohol co-initiator, (*R*)(+)-1-phenylethanol or (*S*)(-)-1-phenylethanol, the isotacticity was further increased to $P_m = 0.85$ (run 11, Table 1) or 0.87 (run 12, Table 1). Noteworthy also is that this high tacticity achieved was accompanied by a perfect (100%) or near-perfect (106%, indicative of some chain transfer events) initiation efficiency. With this high level of isotacticity, the PBiL materials derived from the stereoselective polymerization of *rac*-BiL by the chiral catalyst/initiator system finally became semi-crystalline, as evidenced by their endothermic first-order melting transitions with high T_m values at 150°C and 154°C (Figure 5D).

Mechanisms of stereoselection and stereoerror generation

To shed light on the mechanism of stereoselection by the enantiopure catalyst and the generation of stereoerrors by the racemic catalyst, density functional theory (DFT) calculations were carried out first for the polymerization of BiL as a racemic mixture

**Figure 6. Summary of computational results**(A) Polymerization pathways and energies for the polymerization of *rac*-BiL with enantiopure (S,S)-Y-3.(B) Polymeric chain exchange pathway proposed for the polymerization of *rac*-BiL with *rac*-Y-3 (TS = transition state).

(C) Optimized geometry of the transition state for the dimer formation along the polymer chain exchange pathway. Atoms reported as follows: Y, cyan; O, red; N, blue; C, gray; and H, white. All free energies reported in toluene and kcal/mol.

with (S,S)-Y-3. At first, we investigated the relative stability of (S,S)-Y-3 bearing a (S,R)-chain or a (R,S)-chain, namely (S,S)-Y-3/(S,R)-chain or (S,S)-Y-3/(R,S)-chain propagating sites, and found 1.5 kcal/mol in favor of the (S,S)-Y-3/(R,S)-chain site, indicating a moderate thermodynamic preference for the reactivity of (R,S)-BiL enantiomer with (S,S)-Y-3 catalyst. Next, we investigated the kinetics of BiL insertion into the Y–O chain bond to examine the effect of the monomer chirality on the interaction with the chain end (Figure 6A). Starting from the more stable (S,S)-Y-3/(R,S)-chain propagating sites, insertion of the same enantiomer (R,S)-BiL is preferred over the insertion of the opposite enantiomer (S,R)-BiL by a $\Delta\Delta G^\ddagger$ of 1.5 kcal/mol—activation energies for (R,S)-BiL and (S,R)-BiL insertions are 20.5 and 22.0 kcal/mol, respectively—in good agreement with the experimental P_m of 0.85. When a stereoerror occurs and a (S,R)-chain is formed, the resulting (S,S)-Y-3/(S,R)-chain site then inserts preferentially the (S,R)-BiL monomer over the (R,S)-BiL one by a $\Delta\Delta G^\ddagger$ of 1.2 kcal/mol: activation energies for (R,S)-BiL and (S,R)-BiL insertions are 19.1 and 17.9 kcal/mol, respectively. Overall, these results show that, with an enantiopure catalyst, the polymerization of *rac*-BiL is moderately stereoselective through a combined catalyst-site and chain-end control mechanism, where the catalyst chirality selects the chirality of the chain and, in turn, the chain chirality selects the chirality of the incoming monomer, resulting in a stereoblock-like polymer structure. Any possible polymer chain exchange (*vide infra*) between the (S,S)-Y-3/(R,S)-chain and (S,S)-Y-3/(S,R)-chain sites would have no additional consequences on the polymer microstructures. As switching the chirality of the initiating alcohol, (R or S)-Me(Ph)CHOH, was also found to not affect, noticeably, the tacticity of the resulting PBiL (run 11 versus 12, Table 1), we computed the transition state for insertion of both BiL enantiomers into the (S,S)-Y-OCH(Ph)Me bond. The reaction with (S,S)-Y-(S)-OCH(Ph)Me was favored by ~3.5 kcal/more over the reaction with (S,S)-Y-(R)-OCH(Ph)Me, but this difference is the same for both BiL enantiomers, thus confirming that the initiation step does not select preferentially either enantiomer of the monomer.

To verify the computational result that the chiral catalyst (*S,S*)-Y-3 selectively polymerizes (*R,S*)-BiL over its enantiomer (*S,R*)-BiL, we examined the kinetic profile of the ROP of *rac*-BiL catalyzed by (*S,S*)-Y-3 until it reached to around 50% monomer conversion. The polymerization strictly follows the first-order kinetics (Figure S53). The specific rotation of the residual monomer when the ROP was quenched at 49% conversion was measured to be +19 deg dm⁻¹g⁻¹cm³ in CHCl₃. When compared with the specific rotation of (*R,S*)-BiL, $[\alpha]_{589}^{22.4} = -31$ deg dm⁻¹g⁻¹cm³ in CHCl₃, it can be concluded that the residual monomer pool was (*S,R*)-BiL enriched. Overall, the experimental result agrees with that of the DFT calculation.

Moving to the polymerization by a racemic catalyst mixture, *rac*-Y-3, possible polymer chain exchange between two antipodal catalyst centers carrying opposite chains must now be taken into account. For the exchange to happen without free alcohol, we propose here a mechanism that involves an *intermolecular* transesterification step between the two enantiomers of the catalyst exchanging chains of opposite chiralities, through the formation of a dimeric intermediate (Figure 6B). The two anionic chain ends act as bridges between the two propagating species while maintaining the favored seven-coordinate ligand environment typical of such Y catalysts. Out of all the possible dimeric species that could be formed, we focused on the one having opposite enantiomers of Y-3 and opposite chiral chains, as it is the one that imposes stereomicrostructure consequences in the stereoselective polymerization as a result of polymer chain exchange. Interestingly, this proposed dimeric intermediate (Figure 6B) was found to be more stable than the relative monomeric propagating species, by 2.8 kcal/mol if it dissociates as (*S,S*)-Y-3/(*R,S*)-chain and (*R,R*)-Y-3/(*S,R*)-chain, or by 5.8 kcal/mol if it dissociates as (*S,S*)-Y-3/(*S,R*)-chain and (*R,R*)-Y-3/(*R,S*)-chain. The stability of the dinuclear species could be attributed to possible stabilizing Y-Y interaction (3.8 Å), as compared with the reported Y-Y distances of 3.6–3.7 Å,^{72–74} and μ-alkoxy bridging (Figure S54), which is consistent with the observations that yttrium salen complexes are favored to form dinuclear structures in non-coordinating solvent (e.g., toluene) via alkoxy bridging.^{71,75,76} This analysis suggests that the active site environment is mostly populated as dimers when the majority of the monomer is consumed. In this context, we have summarized the DFT results in Figure 6B by setting this dimeric species as a reference structure at 0 kcal/mol; the transition state for the dimer formation (Figure 6C) was located at 22 kcal/mol above that reference point.

Dissociation of the dimer toward the formation of higher energy monomeric (*S,S*)-Y-3/(*S,R*)-chain and (*R,R*)-Y-3/(*R,S*)-chain sites leads to more reactive but less stereoselective sites than the dissociation toward the lower energy monomeric (*S,S*)-Y-3/(*R,S*)-chain and (*R,R*)-Y-3/(*S,R*)-chain sites, which are less reactive but more stereoselective. Specifically, the transition states for the former combination are lower in energy (17.9 and 19.1 kcal/mol) and less stereoselective ($\Delta\Delta G^\ddagger = 1.2$ kcal/mol) than the latter combination, with the transition states located at higher energies (22.0 and 20.5 kcal/mol) and being more stereoselective ($\Delta\Delta G^\ddagger = 1.5$ kcal/mol). Thus, in the case of polymerization by *rac*-Y-3, polymer chain exchange via dimeric intermediates represents an additional source of stereoerrors, as the process converts two slower and more selective propagating sites into two faster and less selective sites, thus reducing the overall stereoselectivity.

Overall, in the presence of *rac*-Y-3, access to the less stereoselective propagating species can occur either by polymer chain exchange or by inherent addition/insertion errors, accounting for the additional generation of stereoerrors to produce polymers with a low P_m of ~0.45. Hence, understanding of this mechanism provides a

straightforward way of enhancing the stereoselectivity by employing an enantioselective pure catalyst, under which conditions the additional stereoerrors originated from the polymer exchange pathway are eliminated, thereby producing polymers with much higher stereoregularity (*vide supra*).

Thermal and mechanical properties and chemical recyclability

The most marked effect of structural hybridization of the LCT γ -BL with the HCT ϵ -CL that led to the design of the hybrid monomer BiL has been observed on thermal property enhancements. Specifically, the PBiL material derived from the [5+7] hybrid monomer BiL displays a high T_g ranging from 119°C to 135°C (Figures 2C and 5C), thus representing up to 200°C enhancements in T_g in relation to PGBL and PCL homopolymers as well as their copolymers. The T_m of the pure isotactic P[(1*R*, 5*S*)-BiL] was determined to be 263°C (Figure 4B), also reflecting a ~200°C increase in relation to the T_m values of PGBL and PCL as well as their copolymers. The remarkable enhancement trend can be extended to the thermal stability with PBiL (with 18% *trans*) exhibiting a high $T_{d,5\%}$ of 318°C and a high T_{max} of 354°C (Figure 2D), which are about 116°C and 136°C higher than the $T_{d,5\%}$ and T_{max} values of PGBL. The $T_{d,5\%}$ of all *cis*-PBiL with $M_n = 153 \text{ kg mol}^{-1}$ prepared by *rac*-La-2 (run 4, Table 1) showed a further increased $T_{d,5\%}$ to 336°C (Figure 7A), approaching to that of PCL.

Mechanical properties of two PBiL samples, one with all *cis*-chains prepared by *rac*-La-2 ($M_n = 94.3 \text{ kg mol}^{-1}$) and the other with *cis* (82%) and *trans* (18%) prepared by TBD ($M_n = 56.7 \text{ kg mol}^{-1}$), were examined by tensile testing of their dog-bone-shaped specimens. The all-*cis*-PBiL material is best described as a hard, strong, and brittle glass, as characterized by a high Young's modulus ($E = 3.05 \pm 0.18 \text{ GPa}$), a high ultimate tensile strength ($\sigma_B = 53.6 \pm 0.3 \text{ MPa}$), and a low elongation ($\varepsilon_B = 2.2\%$) (Figure 7B). As compared with PGBL ($M_n = 42.5 \text{ kg mol}^{-1}$),⁷⁷ *cis*-PBiL enhanced Young's modulus by ~10× and tensile strength by ~3× but with significantly reduced ductility. A similar trend was found when compared with PCL,⁷⁸ observing enhanced Young's modulus by >10× and tensile strength by ~1.5×. In contrast, the PBiL material with 18% *trans* structure is a plastic, characterized by a yield point, a lower (but still high) E ($2.00 \pm 0.10 \text{ GPa}$), a lower σ_B ($18.9 \pm 3.3 \text{ MPa}$), and a higher ductility ($\varepsilon_B = 85.8\% \pm 23.2\%$). Overall, these results showed that all-*cis*-PBiL is drastically different than its hybridizing parents PGBL and PCL with much higher modulus but much lower ductility, and the results also demonstrated the mechanical properties of PBiL materials can be tuned by introducing some *trans* chains via epimerization.

Another hypothesized unique feature of the HCT/LCT hybrid monomer is that it could exhibit both high polymerizability by virtue of the HCT structural motif and high depolymerizability via the LCT structural fragment, thereby unifying otherwise conflicting properties in a single monomer. To quantify the polymerizability of BiL and the depolymerizability of PBiL as a function of reaction conditions, the thermodynamics of the BiL polymerization were probed by using $[M]/[La-1]/[BnOH] = 100/1/3$ ($M = BiL$) and $[M]_0 = 0.5 \text{ mol L}^{-1}$ in toluene- d_8 via a variable-temperature NMR study. The equilibrium monomer concentration, $[M]_{eq}$, obtained by plotting $[M]_t$ as a function time until $[M]$ became constant, was measured to be 0.293, 0.216, 0.171, 0.127, and 0.0935 mol L⁻¹ for 50, 40, 30, 20°C, and 10°C, respectively. The van't Hoff plot of $\ln[M]_{eq}$ versus 1/T gave a straight line ($R^2 = 0.999$, Figures S45 and S46), from which the thermodynamic parameters were calculated to be $\Delta H_p^\circ = -21.1 \text{ kJ} \cdot \text{mol}^{-1}$ and $\Delta S_p^\circ = -55.8 \text{ J} \cdot \text{mol}^{-1} \cdot \text{K}^{-1}$, based on the equation $\ln[M]_{eq} = \Delta H_p^\circ/RT - \Delta S_p^\circ/R$.⁵³ The T_c value was calculated to be 575 K (302°C) at $[M]_0 = 10.0 \text{ mol L}^{-1}$ or 379 K (106°C) at $[M]_0 = 1.0 \text{ mol L}^{-1}$, based on the equation $T_c = \Delta H_p^\circ / [\Delta S_p^\circ + R \ln[M]_0]$.⁵³ These results

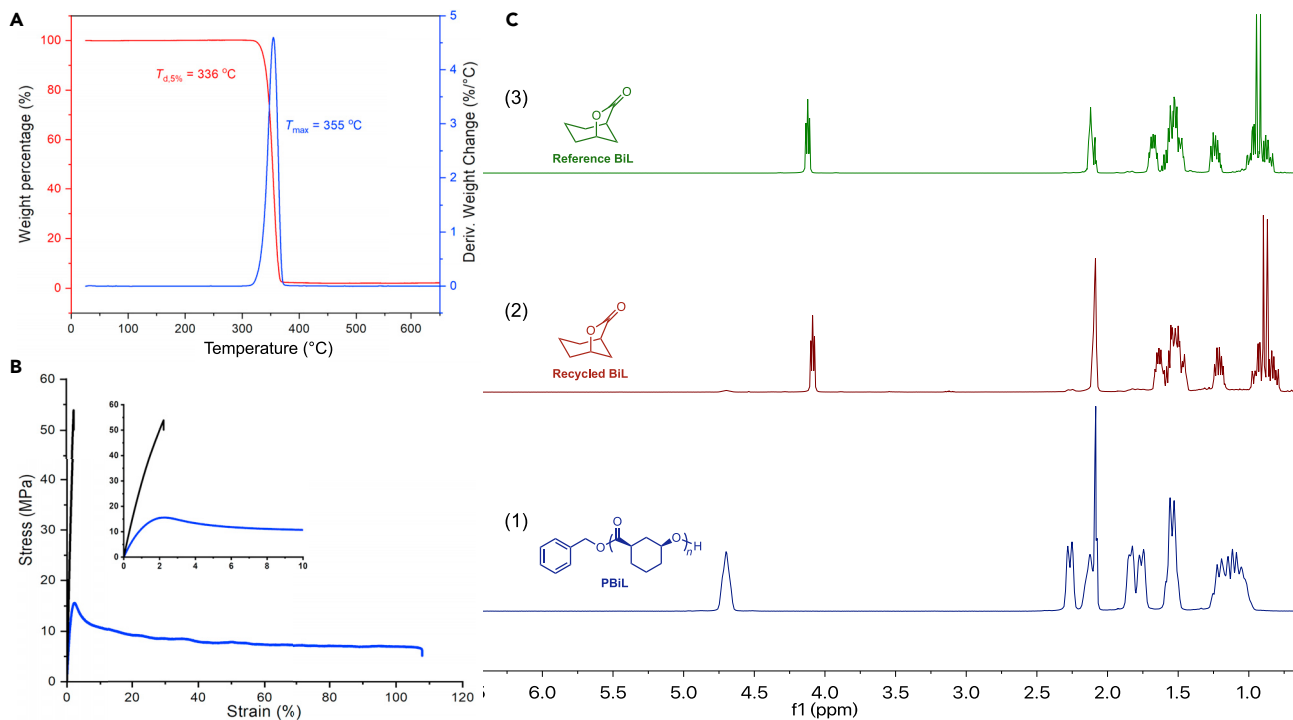


Figure 7. Thermal and mechanical properties and chemical recyclability of PBiL

(A) TGA and DTG thermograms of PBiL ($M_n = 153 \text{ kg mol}^{-1}$, $D = 1.06$) prepared by rac-La-2.

(B) Stress-strain curves for the PBiL prepared by rac-La-2 ($M_n = 94.3 \text{ kg mol}^{-1}$, all cis structure, black curve) and the PBiL prepared by TBD ($M_n = 56.7 \text{ kg mol}^{-1}$, cis (82%) and trans (18%) structures, blue curve). Inset: blowup region from 0% to 10% elongation.

(C) ¹H NMR (toluene-*d*₈) spectra of PBiL ($M_n = 13.1 \text{ kg mol}^{-1}$) prepared by La-1 at RT (1); the recovered monomer BiL obtained after depolymerization by La-1 at 120 °C (2); and the starting monomer BiL for comparison (3).

indicate both good polymerizability of BiL and depolymerizability of PBiL by adjusting the reaction conditions (temperature and concentration).

Consistent with the above derived thermodynamic parameters, the polymerization results summarized in Table 1 showed the relatively high polymerizability of BiL, achieving a high monomer conversion up to 93% at RT and 6.0 M of initial BiL concentration. Next, we probed the depolymerizability of the preformed PBiL by La-1 at RT by using the same catalyst at higher temperatures. Specifically, the depolymerization of PBiL in toluene-*d*₈ was monitored *in situ* by ¹H NMR, revealing that the depolymerization achieved near completion (>95%) after heating at 120 °C for 36 h to regenerate the monomer BiL (Figure 7C). It is worth noting that, when the depolymerization of PBiL prepared by the TBD-catalyzed ROP at RT ($M_n = 56.7 \text{ kg mol}^{-1}$, 82% cis + 18% trans) was performed by using the same basic TBD catalyst at 120 °C, the PBiL underwent further epimerization, whereas only a small amount of BiL was regenerated after 1 h. Nevertheless, when the depolymerization was extended to 12 h, all PBiL, including both cis and trans chains, was completely depolymerized to cleanly recover BiL (Figure S47). This exclusive selectivity for the BiL monomer recovery is possible, despite the fact that base-mediated epimerization can inter-convert the cis and trans chains, because the bridged bicyclic monomer BiL exists only in the cis-configuration, which is fixed by the spatially atom-bridged structure, and the monomer is stable under such base condition (in the absence of initiator). Therefore, PBiL can be completely depolymerized and converted into the most thermodynamically favored state—the monomer state under suitable conditions.

DISCUSSION

The design of useful circular polymers requires building-block monomer structures that can balance conflicting monomer polymerizability, polymer depolymerizability, and polymer performance properties. The herein described HCT/LCT hybrid monomer design synergistically utilizes both the high polymerizability and performance properties of the HCT sub-structural unit and the high depolymerizability of the LCT sub-structural unit, thereby unifying the conflicting properties in a single monomer structure. The mechanism of such hybrid monomers to solve the property trade-offs can be thought of as the intriguing two-pathway scenario wherein the polymerization proceeded via the ring-opening of the HCT sub-structure and the depolymerization occurred through the ring-closing to form the LCT sub-structure.

Even more intriguingly, the thermal and mechanical properties of the polymers derived from the hybridized monomers can be far superior to those homo- or copolymers of the parent monomers. This marked property enhancement has been demonstrated by the prototype example of the hybrid monomer BiL consisting of both HCT ϵ -CL and LCT γ -BL. Specifically on thermal properties, PBiL exhibits a high T_g up to 135°C and T_m up to 263°C, which are \sim 200°C above both the T_g and T_m values of the parent PGBL and PCL as well as their copolymers. On mechanical properties, PBiL also showed a marked enhancement in Young's modulus and tensile strength, displaying \sim 10× higher Young's modulus and \sim 3× higher tensile strength relative to PGBL and $>$ 10× higher modulus and \sim 1.5× higher tensile strength relative to PCL. The HCT/LCT hybrid monomer strategy, as a powerful approach for circular polymer design, which has been demonstrated by the results reported here, could be broadly applicable to designing other monomers that can address property trade-offs within a single monomer structure.

The (de)polymerization chemistry of analogous bicyclic lactones and thiolactones, as well as the properties of their derived corresponding polyesters and polythioesters, can be significantly different. For example, bicyclic thioester^[221]BTL produces crystalline and fully recyclable polythioester PBTL with the unique tacticity-independent crystallinity,⁴² whereas the bicyclic lactone congener gives amorphous and non-recyclable polyester—basically the opposite of PBTL. Three factors count for these large differences. First, with the larger S atom (versus O), the thioester bond is longer than the ester bond, which, together with differences in bond angles, imparts differences in ring strain. Second, the polarity of the carbonyl group in the thioester bond is higher than that in the ester bond, effectively increasing the interactions between polymer chains and, thus, leading to higher T_m values of the polythioester. Third, the conformation of the in-chain cyclopentane ring is also important for PBTL's tolerance of crystallinity toward stereodefects. The current polyester derived from BiL possesses neither the thioester bond nor the in-chain cyclopentane ring, explaining why no unusual tacticity-independent crystallinity was observed.

Computational studies have traced the origin of stereoerrors generated from the stereoselective polymerization of racemic BiL by both enantiopure and racemic catalysts. The derived polymer chain exchange mechanism involves the formation of the surprisingly stable dimeric propagating intermediate between the two enantiomers of the catalyst sites, which provides a pathway for exchanging the chains of opposite chiralities. Dissociation of the dimeric intermediate leads to monomeric propagating sites with more reactive but less stereoselective and less reactive but more stereoselective site combinations. With this mechanism understood, an effective strategy to eliminate such polymer-exchange-induced stereoerrors has been realized by employing a single enantiomer of the catalyst, which significantly enhanced the stereoselectivity of the polymerization.

EXPERIMENTAL PROCEDURES

Resource availability

Lead contact

Requests for further information should be directed to and will be fulfilled by the Lead Contact, Eugene Y.-X. Chen (eugene.chen@colostate.edu).

Materials availability

This study did not generate new unique materials.

Data and code availability

All data needed to evaluate the conclusions in the paper are present in the paper and/or the Supplemental information.

SUPPLEMENTAL INFORMATION

Supplemental information can be found online at <https://doi.org/10.1016/j.chempr.2021.02.003>.

ACKNOWLEDGMENTS

This work was supported in part by Colorado State University (CSU) and by the U.S. Department of Energy, Office of Energy Efficiency and Renewable Energy, Advanced Manufacturing Office (AMO), and Bioenergy Technologies Office (BETO). This work was performed as part of the BOTTLE Consortium, which includes members from CSU, and funded under contract number DE-AC36-08GO28308 with the National Renewable Energy Laboratory, operated by Alliance for Sustainable Energy. The computational study used the resources of the King Abdullah University of Science and Technology Super-Computing Laboratory (KSL).

AUTHOR CONTRIBUTIONS

C.S. and E.Y.-X.C. conceived the idea and designed the experiments. C.S. carried out the experiments, and L.F. and L. Cavallo performed and analyzed the DFT calculations. C.S., L.F., and E.Y.-X.C. co-wrote the manuscript, and all authors participated in data analysis and discussions and read and edited the manuscript. E.Y.-X.C. directed the project.

DECLARATION OF INTERESTS

E.Y.-X.C. and C.S. are inventors on a U.S. provisional application submitted by Colorado State University Research Foundation, which covers the herein described polymers. All other authors declare no competing interests.

Received: October 23, 2020

Revised: December 23, 2020

Accepted: February 1, 2021

Published: March 11, 2021

REFERENCES

1. Jambeck, J.R., Geyer, R., Wilcox, C., Siegler, T.R., Perryman, M., Andrady, A., Narayan, R., and Law, K.L. (2015). Marine pollution. Plastic waste inputs from land into the ocean. *Science* 347, 768–771.
2. Geyer, R., Jambeck, J.R., and Law, K.L. (2017). Production, use, and fate of all plastics ever made. *Sci. Adv.* 3, e1700782.
3. Lamb, J.B., Willis, B.L., Fiorenza, E.A., Couch, C.S., Howard, R., Rader, D.N., True, J.D., Kelly, L.A., Ahmad, A., Jompa, J., and Harvell, C.D. (2018). Plastic waste associated with disease on coral reefs. *Science* 359, 460–462.
4. World Economic Forum (2016). The new plastics economy: rethinking the future of plastics (Ellen MacArthur foundation and McKinsey & company). <https://www.ellenmacarthurfoundation.org/publications/the-new-plastics-economy-rethinking-the-future-of-plastics>.
5. US Department of Energy (2020). Report of the basic energy sciences roundtable on chemical upcycling of polymers, April 30–May 1, 2019. <https://science.osti.gov/-/media/bes/pdf/>

- reports/2020/Chemical_Upcycling_Polymers.pdf.
6. National Academies of Sciences, Engineering, and Medicine (2020). Closing the loop on the plastics dilemma proceedings of the a workshop in brief (The National Academies Press). <https://doi.org/10.17226/25647>.
 7. Scheutz, G.M., Lessard, J.J., Sims, M.B., and Sumerlin, B.S. (2019). Adaptable crosslinks in polymeric materials: resolving the intersection of thermoplastics and thermosets. *J. Am. Chem. Soc.* 141, 16181–16196.
 8. Garcia, J.M., and Robertson, M.L. (2017). The future of plastics recycling. *Science* 358, 870–872.
 9. Hillmyer, M.A. (2017). The promise of plastics from plants. *Science* 358, 868–870.
 10. Zhu, Y., Romain, C., and Williams, C.K. (2016). Sustainable polymers from renewable resources. *Nature* 540, 354–362.
 11. Zhang, X., Fevre, M., Jones, G.O., and Waymouth, R.M. (2018). Catalysis as an enabling science for sustainable polymers. *Chem. Rev.* 118, 839–885.
 12. Rorrer, N.A., Nicholson, S., Carpenter, A., Biddy, M.J., Grundl, N.J., and Beckham, G.T. (2019). Combining reclaimed PET with bio-based monomers enables plastics upcycling. *Joule* 3, 1006–1027.
 13. Yoshida, S., Hiraga, K., Takehana, T., Taniguchi, I., Yamaji, H., Maeda, Y., Toyohara, K., Miyamoto, K., Kimura, Y., and Oda, K. (2016). A bacterium that degrades and assimilates poly(ethylene terephthalate). *Science* 351, 1196–1199.
 14. Tournier, V., Topham, C.M., Gilles, A., David, B., Folgoas, C., Moya-Leclair, E., Kamionka, E., Desrousseaux, M.L., Texier, H., Gavalda, S., et al. (2020). An engineered PET depolymerase to break down and recycle plastic bottles. *Nature* 580, 216–219.
 15. Jia, X., Qin, C., Friedberger, T., Guan, Z., and Huang, Z. (2016). Efficient and selective degradation of polyethylenes into liquid fuels and waxes under mild conditions. *Sci. Adv.* 2, e1501591.
 16. Rahimi, A., and García, J.M. (2017). Chemical recycling of waste plastics for new materials production. *Nat. Rev. Chem.* 1, 0046.
 17. Schneiderman, D.K., and Hillmyer, M.A. (2017). 50th anniversary perspective: there is a great future in sustainable polymers. *Macromolecules* 50, 3733–3749.
 18. Lu, X.B., Liu, Y., and Zhou, H. (2018). Learning nature: recyclable monomers and polymers. *Chemistry* 24, 11255–11266.
 19. Jehanno, C., Pérez-Madrigal, M.M., Demarteau, J., Sardon, H., and Dove, A.P. (2019). Organocatalysis for depolymerisation. *Polym. Chem.* 10, 172–186.
 20. Tang, X., and Chen, E.Y.-X. (2019). Toward infinitely recyclable plastics derived from renewable cyclic esters. *Chem* 5, 284–312.
 21. Zhu, J.B., Watson, E.M., Tang, J., and Chen, E.Y.-X. (2018). A synthetic polymer system with repeatable chemical recyclability. *Science* 360, 398–403.
 22. Zhu, J.B., and Chen, E.Y.-X. (2019). Catalyst-sidearm-induced stereoselectivity switching in polymerization of a racemic lactone for stereocomplexed crystalline polymer with a circular life cycle. *Angew. Chem. Int. Ed. Engl.* 58, 1178–1182.
 23. Shi, C.-X., Guo, Y.-T., Wu, Y.-H., Li, Z.-Y., Wang, Y.-Z., Du, F.-S., and Li, Z.-C. (2019). Synthesis and controlled organobase-catalyzed ring-opening polymerization of morpholine-2,5-dione derivatives and monomer recovery by acid-catalyzed degradation of the polymers. *Macromolecules* 52, 4260–4269.
 24. MacDonald, J.P., and Shaver, M.P. (2016). An aromatic/aliphatic polyester prepared via ring-opening polymerisation and its remarkably selective and cyclable depolymerisation to monomer. *Polym. Chem.* 7, 553–559.
 25. Yuan, J., Xiong, W., Zhou, X., Zhang, Y., Shi, D., Li, Z., and Lu, H. (2019). 4-Hydroxyproline-derived sustainable polythioesters: controlled ring-opening polymerization, complete recyclability, and facile functionalization. *J. Am. Chem. Soc.* 141, 4928–4935.
 26. Lloyd, E.M., Lopez Hernandez, H., Feinberg, E.C., Yourdkhani, M., Zen, E.K., Mejia, E.B., Sottos, N.R., Moore, J.S., and White, S.R. (2019). Fully recyclable metastable polymers and composites. *Chem. Mater.* 31, 398–406.
 27. Kaitz, J.A., Lee, O.P., and Moore, J.S. (2015). Depolymerizable polymers: preparation, applications, and future outlook. *MRS Commun.* 5, 191–204.
 28. Christensen, P.R., Scheuermann, A.M., Loeffler, K.E., and Helms, B.A. (2019). Closed-loop recycling of plastics enabled by dynamic covalent diketoneamine bonds. *Nat. Chem.* 11, 442–448.
 29. García, J.M., Jones, G.O., Virwani, K., McCloskey, B.D., Boddy, D.J., ter Huurne, G.M., Horn, H.W., Coady, D.J., Bintaleb, A.M., Alabdulrahman, A.M.S., et al. (2014). Recyclable, strong thermosets and organogels via paraformaldehyde condensation with diamines. *Science* 344, 732–735.
 30. Liu, Y., Zhou, H., Guo, J.Z., Ren, W.M., and Lu, X.B. (2017). Completely recyclable monomers and polycarbonate: approach to sustainable polymers. *Angew. Chem. Int. Ed. Engl.* 56, 4862–4866.
 31. Lizundia, E., Makwana, V.A., Larrañaga, A., Vilas, J.L., and Shaver, M.P. (2017). Thermal, structural and degradation properties of an aromatic-aliphatic polyester built through ring-opening polymerisation. *Polym. Chem.* 8, 3530–3538.
 32. Schneiderman, D.K., Vanderlaan, M.E., Mannion, A.M., Panthani, T.R., Batiste, D.C., Wang, J.Z., Bates, F.S., Macosko, C.W., and Hillmyer, M.A. (2016). Chemically recyclable biobased polyurethanes. *ACS Macro Lett.* 5, 515–518.
 33. Diesendruck, C.E., Peterson, G.I., Kulik, H.J., Kaitz, J.A., Mar, B.D., May, P.A., White, S.R., Martínez, T.J., Boydston, A.J., and Moore, J.S. (2014). Mechanically triggered heterolytic unzipping of a low-ceiling-temperature polymer. *Nat. Chem.* 6, 623–628.
 34. Hong, M., and Chen, E.Y.-X. (2017). Chemically recyclable polymers: a circular economy approach to sustainability. *Green Chem.* 19, 3692–3706.
 35. Hong, M., and Chen, E.Y.-X. (2019). Future directions for sustainable polymers. *Trends in Chemistry* 1, 148–151.
 36. Coates, G.W., and Getzler, Y.D.Y.L. (2020). Chemical recycling to monomer for an ideal, circular polymer economy. *Nat. Rev. Mater.* 5, 501–516.
 37. Olsén, P., Odelius, K., and Albertsson, A.C. (2016). Thermodynamic presynthetic considerations for ring-opening polymerization. *Biomacromolecules* 17, 699–709.
 38. Schneiderman, D.K., and Hillmyer, M.A. (2016). Aliphatic polyester block polymer design. *Macromolecules* 49, 2419–2428.
 39. Hong, M., and Chen, E.Y.X. (2016). Completely recyclable biopolymers with linear and cyclic topologies via ring-opening polymerization of γ -butyrolactone. *Nat. Chem.* 8, 42–49.
 40. Hong, M., and Chen, E.Y.-X. (2016). Towards truly sustainable polymers: a metal-free recyclable polyester from biorenewable non-strained γ -butyrolactone. *Angew. Chem. Int. Ed. Engl.* 55, 4188–4193.
 41. Sangroniz, A., Zhu, J.B., Tang, X., Etxeberria, A., Chen, E.Y.X., and Sardon, H. (2019). Packaging materials with desired mechanical and barrier properties and full chemical recyclability. *Nat. Commun.* 10, 3559.
 42. Shi, C., McGraw, M.L., Li, Z.C., Cavallo, L., Falivene, L., and Chen, E.Y.-X. (2020). High-performance pan-tactic polythioesters with intrinsic crystallinity and chemical recyclability. *Sci. Adv.* 6, eabc0495.
 43. Xiong, W., Chang, W., Shi, D., Yang, L., Tian, Z., Wang, H., Zhang, Z., Zhou, X., Chen, E.-Q., and Lu, H. (2020). Geminal dimethyl substitution enables controlled polymerization of penicillamine-derived β -thiolactones and reversed depolymerization. *Chem* 6, 1831–1843.
 44. Tang, X., Westlie, A.H., Watson, E.M., and Chen, E.Y.-X. (2019). Stereosequenced crystalline polyhydroxalkanoates from diastereomeric monomer mixtures. *Science* 366, 754–758.
 45. Tang, X., Westlie, A.H., Caporaso, L., Cavallo, L., Falivene, L., and Chen, E.Y.-X. (2020). Biodegradable polyhydroxalkanoates by stereoselective copolymerization of racemic diolides: stereocontrol and polyolefin-like properties. *Angew. Chem. Int. Ed. Engl.* 59, 7881–7890.
 46. Xu, Y.-C., Ren, W.-M., Zhou, H., Gu, G.-G., and Lu, X.-B. (2017). Functionalized polyesters with tunable degradability prepared by controlled ring-opening (co)polymerization of lactones. *Macromolecules* 50, 3131–3142.
 47. Wilson, J.A., Hopkins, S.A., Wright, P.M., and Dove, A.P. (2015). Synthesis of ω -pentadecalactone copolymers with independently tunable thermal and degradation behavior. *Macromolecules* 48, 950–958.
 48. Hakkarainen, M., Höglund, A., Odelius, K., and Albertsson, A.C. (2007). Tuning the release rate

- of acidic degradation products through macromolecular design of caprolactone-based copolymers. *J. Am. Chem. Soc.* 129, 6308–6312.
49. Tabata, Y., and Abe, H. (2014). Synthesis and Properties of alternating copolymers of 3-hydroxybutyrate and lactate units with different stereocompositions. *Macromolecules* 47, 7354–7361.
50. Wilson, J.A., Hopkins, S.A., Wright, P.M., and Dove, A.P. (2016). Dependence of copolymer sequencing based on lactone ring size and ϵ -substitution. *ACS Macro Lett* 5, 346–350.
51. Wilson, J.A., Hopkins, S.A., Wright, P.M., and Dove, A.P. (2015). Synthesis and postpolymerization modification of one-pot ω -pentadecalactone block-like copolymers. *Biomacromolecules* 16, 3191–3200.
52. Labet, M., and Thielemans, W. (2009). Synthesis of polycaprolactone: a review. *Chem. Soc. Rev.* 38, 3484–3504.
53. Duda, A., and Kowalski, A. (2009). Thermodynamics and kinetics of ring-opening polymerization. In *Handbook of Ring-Opening Polymerization*, P. Dubois, O. Coulembier, and J.-M. Raquez, eds. (Wiley-VCH Verlag), pp. 1–51.
54. He, F., Li, S., Garreau, H., Vert, M., and Zhuo, R. (2005). Enzyme-catalyzed polymerization and degradation of copolymers of ϵ -caprolactone and γ -butyrolactone. *Polymer* 46, 12682–12688.
55. Agarwal, S., and Xie, X. (2003). SmI₂/Sm-based γ -butyrolactone– ϵ -caprolactone copolymers: microstructural characterization using one- and two-dimensional NMR spectroscopy. *Macromolecules* 36, 3545–3549.
56. Du, G., Wei, Y., Zhang, W., Dong, Y., Lin, Z., He, H., Zhang, S., and Li, X. (2013). Bis(imino) diphenylamido rare-earth metal dialkyl complexes: synthesis, structure, and catalytic activity in living ring-opening ϵ -caprolactone polymerization and copolymerization with γ -butyrolactone. *Dalton Trans.* 42, 1278–1286.
57. Duda, A., Penczek, S., Dubois, P., Mecerreyes, D., and Jérôme, R. (1996). Oligomerization and copolymerization of γ -butyrolactone — a monomer known as unable to homopolymerize, I. Copolymerization with ϵ -caprolactone. *Macromol. Chem. Phys.* 197, 1273–1283.
58. Hong, M., Tang, X., Newell, B.S., and Chen, E.Y.-X. (2017). “Nonstrained” γ -butyrolactone-based copolymers: copolymerization characteristics and composition-dependent (thermal, eutectic, cocrystallization, and degradation) properties. *Macromolecules* 50, 8469–8479.
59. Shieh, P., Zhang, W., Husted, K.E.L., Kristufek, S.L., Xiong, B., Lundberg, D.J., Lem, J., Veysset, D., Sun, Y., Nelson, K.A., et al. (2020). Cleavable comonomers enable degradable, recyclable thermoset plastics. *Nature* 583, 542–547.
60. Yu, X., Jia, J., Xu, S., Lao, K.U., Sanford, M.J., Ramakrishnan, R.K., Nazarenko, S.I., Hoye, T.R., Coates, G.W., and DiStasio, R.A. (2018). Unraveling substituent effects on the glass transition temperatures of biorenewable polyesters. *Nat. Commun.* 9, 2880.
61. Xu, Y., ucu, T., Perry, M.R., and Shaver, M.P. (2020). Alicyclic polyesters from a bicyclic 1,3-dioxane-4-one. *Polym. Chem.* 11, 4928–4932.
62. Kamber, N.E., Jeong, W., Waymouth, R.M., Pratt, R.C., Lohmeijer, B.G.G., and Hedrick, J.L. (2007). Organocatalytic ring-opening polymerization. *Chem. Rev.* 107, 5813–5840.
63. Kiesewetter, M.K., Shin, E.J., Hedrick, J.L., and Waymouth, R.M. (2010). Organocatalysis: opportunities and challenges for polymer synthesis. *Macromolecules* 43, 2093–2107.
64. Dove, A.P. (2012). Organic catalysis for ring-opening polymerization. *ACS Macro Lett* 1, 1409–1412.
65. Chen, E.Y.X. (2009). Coordination polymerization of polar vinyl monomers by single-site metal catalysts. *Chem. Rev.* 109, 5157–5214.
66. O’Keefe, B.J., Hillmyer, M.A., and Tolman, W.B. (2001). Polymerization of lactide and related cyclic esters by discrete metal complexes. *J. Chem. Soc. Dalton Trans.* 2001, 2215–2224.
67. Pratt, R.C., Lohmeijer, B.G.G., Long, D.A., Waymouth, R.M., and Hedrick, J.L. (2006). Triazabicyclodecene: a simple bifunctional organocatalyst for acyl transfer and ring-opening polymerization of cyclic esters. *J. Am. Chem. Soc.* 128, 4556–4557.
68. Chuma, A., Horn, H.W., Swope, W.C., Pratt, R.C., Zhang, L., Lohmeijer, B.G.G., Wade, C.G., Waymouth, R.M., Hedrick, J.L., and Rice, J.E. (2008). The reaction mechanism for the organocatalytic ring-opening polymerization of l-lactide using a guanidine-based catalyst: hydrogen-bonded or covalently bound? *J. Am. Chem. Soc.* 130, 6749–6754.
69. Zhang, X., Jones, G.O., Hedrick, J.L., and Waymouth, R.M. (2016). Fast and selective ring-opening polymerizations by alkoxides and thioureas. *Nat. Chem.* 8, 1047–1053.
70. Tang, X., and Chen, E.Y.X. (2018). Chemical synthesis of perfectly isotactic and high melting bacterial poly(3-hydroxybutyrate) from bio-sourced racemic cyclic diolide. *Nat. Commun.* 9, 2345.
71. Ovitt, T.M., and Coates, G.W. (2002). Stereosechemistry of lactide polymerization with chiral catalysts: new opportunities for stereocontrol using polymer exchange mechanisms. *J. Am. Chem. Soc.* 124, 1316–1326.
72. Pan, C., Shen, W., Yang, L., Bao, L., Wei, Z., Jin, P., Fang, H., Xie, Y., Akasaka, T., and Lu, X. (2019). Crystallographic characterization of Y₂C_{2n} (2n = 82, 88–94): direct Y–Y bonding and cage-dependent cluster evolution. *Chem. Sci.* 10, 4707–4713.
73. Popov, A.A., Avdoshenko, S.M., Pendás, A.M., and Dunsch, L. (2012). Bonding between strongly repulsive metal atoms: an oxymoron made real in a confined space of endohedral metallofullerenes. *Chem. Commun.* 48, 8031–8050.
74. Xu, L., Xia, C.-J., Wang, L.-F., Xie, L., Wang, B., Zhang, Y.-F., and Huang, X. (2014). Structural evolution, sequential oxidation and chemical bonding in tri- γ -yttrium oxide clusters: Y₃Ox– and Y₃O_x (x = 0–6). *RSC Adv* 4, 60270–60279.
75. Wu, B., Gallucci, J.C., Parquette, J.R., and RajanBabu, T.V. (2014). Bimetallic catalysis in the highly enantioselective ring-opening reactions of aziridines. *Chem. Sci.* 5, 1102–1117.
76. Gu, W., Xu, P., Wang, Y., Yao, Y., Yuan, D., and Shen, Q. (2015). Synthesis and characterization of yttrium and ytterbium complexes supported by salen ligands and their catalytic properties for rac-lactide polymerization. *Organometallics* 34, 2907–2916.
77. Zhang, C.-J., Hu, L.-F., Wu, H.-L., Cao, X.-H., and Zhang, X.-H. (2018). Dual organocatalysts for highly active and selective synthesis of linear poly(γ -butyrolactone)s with high molecular weights. *Macromolecules* 51, 8705–8711.
78. Moore, T., Adhikari, R., and Gunatillake, P. (2005). Chemosynthesis of bioresorbable poly(γ -butyrolactone) by ring-opening polymerisation: a review. *Biomaterials* 26, 3771–3782.